 doi:10.20944/preprints202204.0079.v1

Article

Glucose Starvation or Pyruvate Dehydrogenase Activation Induce A Broad, ERK5-Mediated, Metabolic Remodeling Leading to Fatty Acid Oxidation

Abrar Ul Haq Khan1*, Hamideh Salehi2, Catherine Alexia1, Jose M. Valdivielso3, Milica Bozic3, Isabel C. Lopez-Mejia4, Lluis Fajas4, 5, Sabine Gerbal-Chaloin1, Martine Daujat-Chavanieu1,7, Delphine Gitenay1 and Martin Villalba1,6, 7, *.

1 IRMB, Univ Montpellier, INSERM, Montpellier, France.
2 LBN, University of Montpellier, Montpellier, France
3 Vascular and Renal Translational Research Group. Institut de Recerca Biomedica de Lleida (IRBLLIDA). Lleida, Spain.
4 Center for Integrative Genomics, University of Lausanne, Lausanne, CH-1015, Switzerland.
5 Inserm, Montpellier, France.
6 Institut du Cancer Avignon-Provence Sainte Catherine, Avignon, FRANCE
7 IRMB, Univ Montpellier, INSERM, CNRS, CHU Montpellier, Montpellier, France.
* Correspondence: Martin Villalba (martin.villalba@inserm.fr)

Abstract: Cells have metabolic flexibility that allows them to adapt to changes in substrate availability. Two highly relevant metabolites are glucose and fatty acids (FA), and hence, glycolysis and fatty acid oxidation (FAO) are key metabolic pathways leading to energy production. Both pathways affect each other, and in the absence of one substrate, metabolic flexibility allows cells to maintain sufficient energy production. Here we show that glucose starvation or sustained pyruvate dehydrogenase (PDH) activation by dichloroacetate (DCA) induce a large genetic remodeling to propel FAO. The extracellular signal-regulated kinase 5 (ERK5) is a key effector of this multistep metabolic remodeling. First, there is an increase in the lipid transport by expression of low-density lipoprotein receptor-related proteins (LRP), e.g. CD36, LRP1 and others. Second, an increase of the expression of members of the acyl-CoA synthetase long-chain (ACSL) family activates FA. Finally, the expression of the enzymes that catalyze the initial step in each cycle of FAO, i.e. the acyl-CoA dehydrogenases (ACADs), is induced. All of these pathways lead to enhanced cellular FAO. In summary, we show here that different families of enzymes, which are essential to perform FAO, are regulated by the signaling pathway, i.e. MEK5/ERK5, which transduces changes from the environment to genetic adaptations.

Keywords: fatty acid oxidation; glycolysis; ERK5; metabolic flexibility; metabolic plasticity

1. Introduction

Cells adapt to changing environment by adjusting their metabolism[1]. An initial plastic adaptation should be compensated or reinforced by genetic means to allow long-term fitness in the new environment [1]. A prototype of adaption is the metabolic rewiring of mammalian cells during changes in substrate and/or oxygen availability. This is known as metabolic flexibility and complements metabolic plasticity, which resumes the series of metabolic phenotypes present in a cell. A situation where metabolic flexibility and plasticity have largely been investigated is the Warburg effect, a process by which tumor cells produce lactate from glucose, instead of fully oxidizing it, even in the presence of ample amounts of oxygen [2].

Two of the main metabolic pathways leading to energy production are glycolysis and fatty acid oxidation (FAO) [3]. Oxidation of either glucose or fatty acids (FA) may preponderate depending of nutritional and/or physiologic conditions. Logically both pathways

 doi:10.20944/preprints202204.0079.v1

affect each other, with lipolysis inhibiting glycolysis and glycolysis decreasing FAO [3]. It is expected that inhibition of one pathway will stimulate the other, and interestingly, Hsieh and colleagues have shown in yeast that glucose starvation induces fat metabolism genes [4].

Dichloroacetate (DCA), a pyruvate dehydrogenase kinase 1 (PDK1) inhibitor, inhibits glycolysis and favors oxidative phosphorylation (OXPHOS) [5]. DCA was used to control lactic acidosis [6] and some trials suggested its value also in hypercholesterolemia treatment [7]. DCA controls cholesterol homeostasis [8] and lipid hepatic metabolism in septic mice [9]. Indeed, it decreases plasma cholesterol and triglyceride (TG) levels in animal models and humans [10]. This effect is consecutive to an increase on TG oxidation [11]. Clinical trials with DCA showed interesting results on cholesterol levels however its use was discontinued due to a reversible neuropathological toxicity [12,13]. By promoting OXPHOS, DCA activates the extracellular signal-regulated kinase 5 (ERK5) pathway that turns on the transcription factor family MEF2 [14]. MEF2 binds to the LDLR promoter, inducing de novo LDLR expression, which is responsible of sequestering cholesterol into cells [8]. Other physiological effects of DCA are mediated by ERK5, also mainly through MEF2 activation [15,16]. Although ERK5 also has its own transcriptional domain, it translates stress signals, including metabolic stress, to gene expression through MEF2 [17–20], [21]. ERK5 plays key roles multiple cellular functions [20], including on cell metabolism [22] and to some extent in the control of lipid metabolism [23–25]. This could explain the role of ERK5 in atherosclerosis [19,24,26,27], a disease in which cholesterol levels constitute a risk factor. In this study, we set to determine if ERK5 could be a good candidate to modulate metabolic flexibility by sensing glucose starvation and preparing cells to switch to FAO.

2. Materials and Methods

Ethical statement:

Experimental procedures were conducted according to the European guidelines for animal welfare (2010/63/EU). Protocols were approved by the Animal Care and Use Committee "Languedoc-Roussillon" (approval number: CEEA-LR-12163). All methods were carried out in accordance with the approved guidelines and regulations of this committee.

In vivo mouse experiments:

B6 wt mice were treated with a daily single dose of DCA (50 mg/kg/day) intraperitoneally and mouse mRNA was analyzed in spleen and liver at different time points.

Experiments involving engraftment of AML cells were carried out using 6 to 8 weeks/old male NSG mice as previously described [14,16,23]. For engraftment of human cells, 1 million AML cells were injected intravenously (i.v.) through the lateral tail vein in non-irradiated mice. NSG mice with established human AML tumors (day 80 post-graft) were treated with DCA (50 mg/kg, 1 dose/day by gavage, starting at day 1 for 16 consecutive days). Human tumor AML cells gather in mouse spleen and bone marrow, hence we isolated mRNA from these organs. We used human-specific primers to visualize expression of human mRNA.

For the high fat diet experiments, C57BL/6J mice (12 weeks old were bred and housed in pathogen-free conditions in the animal facility of the University of Lleida (Lleida, Spain). Animals were kept in a 12-hour light/dark cycle at 22° C with ad libitum access to food and water. At 12 weeks of age, mice were placed on a high fat diet (HFD) or ´´Paigen diet´´ (1.25% Cholesterol, 0.5% Cholic acid, 15% Cocoa butter, 1% Corn oil, S9358-E030, Ssniff, Germany) for 4 weeks. Two weeks after the beginning of HFD feeding, mice were subjected to daily injections of sodium dichloroacetate (Santa Cruz, sc-203275) (50 mg/kg/day), intraperitoneally, during the following 2 weeks of the experiment. Mouse experiments performed in this study were approved by the Ethic Committee of the University of Lleida in accordance with the guidelines of European Research Council for the care and use of laboratory animals. Body weight was measured every week from the

Preprints (www.preprints.org) | NOT PEER-REVIEWED | Posted: 8 April 2022 doi:10.20944/preprints202204.0079.v1

beginning of the experiment. Individual food intake was measure after 4 weeks of the experiment. At the end of the experiment, blood was collected by cardiac puncture after a 16-hour overnight fast. The animals were perfused with PBS through a puncture in the left ventricle and organs were harvested.

Cell lines and culture conditions:

The leukemic human cell lines T Jurkat Tag, which carries the SV40 large T Ag, and OCI-AML3 were grown in RPMI 1640–Glutamax (GIBCO) supplemented with 5% (Jurkat) or 10% (OCI-AML3) FBS. The primary cell line (BCL-P2) that we derived from a B-cell lymphoma patient [28] were grown in the same medium with 10% FBS. In certain experiments cells were grown in RPMI 1640 without glucose (GIBCO 11879) with the addition of 2 mM glutamine and 10 mM galactose (OXPHOS medium). HepG2, HepG2-C3A and HuH7 cells were grown in MEM and DMEM respectively supplemented with FBS, sodium pyruvate, glutamine, penicillin and streptomycin. Cellular confluence during experiments was between 80–85%.

Glucose starvation

Cells were washed once in cells RPMI 1640 without glucose (GIBCO 11879) and were grown in the same medium with the addition of 2 mM glutamine and 10 mM galactose (OXPHOS medium).

Human liver samples and preparation of PHHs cultures:

Liver samples were obtained from liver resections performed in adult patients for medical reasons. Human hepatocytes isolation and culture were performed as described previously [29]. Briefly, after liver perfusion, hepatocytes were counted, and cell viability was assessed by trypan blue exclusion test. A suspension of 1 × 106 cells/mL per well was added in 12-well plates pre-coated with type I collagen (Beckton Dickinson) and cells were allowed to attach for 12 hours. Then, the supernatant containing dead cells and debris was carefully removed and replaced with 1 mL of serum-free long-term culture medium (Lanford medium, LNF). The number of confluent attached cells was estimated at ~1.5 × 105 cells/cm2.

Reagents and antibodies:

DCA was from Santa Cruz Technologies. Galactose and glutamine were from GIBCO. Human anti-CD36-PE, anti-CD36L-PE, anti-LPR1-PE and IgG were from BD Biosciences and 7AAD from Beckman. The MEK5 inhibitor BIX02189 and the ERK5 inhibitor XMD8–92 were from Selleck. RIPA buffer to prepare protein extracts was from Euromedex. The complete protease inhibitor cocktail (Complete EDTA-free) and the phosphatase inhibitor cocktail (PhosSTOP) were from Roche. ERK5, ACDVL and MEF2A/C antibodies were from Cell Signaling Technology and Abcam respectively. The antibody against β-Actin and HRP-labeled secondary antibodies were from Sigma.

Transient transfection:

Jurkat cells in logarithmic growth phase were transfected with the indicated amounts of plasmid by electroporation. In each experiment, cells were transfected with the same total amount of DNA by supplementing with empty vector. Cells were incubated for 10 min at RT with the DNA mix and electroporated using the Gene Pulser Xcell™ Electroporation system (Bio-Rad) at 260 mV, 960 mF in 400 µl of RPMI 1640. Expression of the different proteins was confirmed by western blot. The transfection efficiency in Jurkat TAg cells is between 60 and 80%. OC-AML-3 cells were transfected using Amaxa TM D-Nucleofector TM Lonza Kit according to manufactured protocol. In HuH7 and HCT116 cells, transfection of 30–50 nM siRNAs was carried out using Lipofectamine RNAiMAX (Invitrogen) in Opti-MEM (Invitrogen), according to the manufacturer's instructions.

 doi:10.20944/preprints202204.0079.v1

Primary hepatocytes were transfected twice at days 1 and 3 post-seeding. Cells were harvested 48 to 96 h post-transfection.

Plasmids:

The expression vectors for ERK5, the pSUPER expression vector for GFP alone or GFP plus shERK5 and the pSiren-retroQ-puro (BD Biosciences) retroviral vectors for shERK5 and control have been previously described [30]. Control, MEF2A and C and ERK5 siRNA were ON-TARGETplus SMARTpools (mixture of 4 siRNA) were from Dharmacon.

Counting and determination of cell viability:

Cell number, viability and cell death was analyzed with the Muse Cell Analyzer (Millipore) by incubating cells with Muse Count & Viability and Annexin V and Dead Cell kits respectively, following manufacturer's instructions.

RT-QPCR:

Total RNA was extracted using NucleoSpin RNA isolation columns (Macherey-Nagel), reverse transcription was carried out using iScript™ cDNA Synthesis Kit (Biorad). Quantitative PCR was performed with KAPA SYBR Green qPCR SuperMix (Cliniscience) and a CFX Connect™ Real-Time qPCR machine (Biorad). All samples were normalized to β-actin mRNA levels. Results are expressed relative to control values arbitrarily set at 100.

Immunoblotting:

Protein analysis by immunoblotting was performed essentially. Briefly, samples were collected, washed out with PBS and lysed with RIPA buffer. Protein concentration was determined by BCA assay (Pierce) before electrophoresis in 4–15% TGX gels (BioRad) and equal amount of protein was loaded in each well. Protein transfer was performed in TransTurbo system (BioRad) in PVDF membranes. After blocking for 1 h with 5% non-fat milk, membranes were incubated overnight at 4 °C in agitation with primary antibodies, washed three times with PBS-Tween 0,1% and incubated with the appropriate HRP-labeled secondary antibody for 1 h. Membranes were washed out three times with PBS-Tween 0,1% and developed with Substrat HRP Immobilon Western (Millipore). Band quantification was performed using the "ImageLab" software from BioRad and represented as the ratio between the protein of interest and a control protein i.e., actin. The value of 1 is arbitrarily given to control cells. One blot representative of several experiments is shown.

Cellular lipid uptake:

Following treatment with DCA or OXPHOS medium, cells were incubated with BODIPYTM FL-C12 (Dodecanoic Acid) or BODIPYTM FL-C16 (Hexadecanoic Acid) form InvitrogenTM in PBS with 2% FBS and incubated at 37 °C for 30 min. Cells were then washed and suspended in 200–250 µl PBS 2% FBS and fluorescence was analyzed using Gallios flow cytometer (Beckman) and the Kaluza software.

Serum triglycerides

They were determined by standard clinical methods using a multichannel Hitachi Modular analyzer (Roche Diagnostics, Indianapolis, USA).

Extracellular Flux Analysis

Mitochondrial respiration and glycolysis was evaluated by using the XF24 Flux analyzer (SeaHorse Bioscience), which measures oxygen consumption rate (OCR) and extracellular acidification rate (ECAR). HCT116 were treated with 5 mM DCA over 72 h (48 h in a 10 cm plate, and the last 24 h in the seahorse plate). To account for differences in cell

Preprints (www.preprints.org) | NOT PEER-REVIEWED | Posted: 8 April 2022 doi:10.20944/preprints202204.0079.v1

proliferation, 8.000 cells were seeded per well in the DCA treatment condition, 7500 cells in the control conditions the day before OCR assay in the Seahorse XF24. OCR measurement was performed in XF media (nonbuffered DMEM) supplemented with 2.5 mM glucose, 2 mM L-glutamine and 1 mM sodium pyruvate, under basal conditions and in response to mitochondrial inhibitors: 1 mM oligomycin, 0.33 mM FCCP, 100 nM rotenone and 1 mM antimycin A (Sigma). OCR, in pMoles/min, was measured during 4 min. The basal respiration rate is calculated as the difference between basal OCR and OCR after inhibition of mitochondrial complex 1 and 3 with rotenone and antimycin A, respectively. The maximum respiration rate was measured following addition of the uncoupler FCCP (uncoupled rate), indicative of the maximum activity of electron transport and substrate oxidation achievable by the cells. To assess fatty acid oxidation involvement in OCR, cells were treated with 5 μM etomoxir 1 hour prior flux analyses.

For the glycolysis assay (Figure 5B), HepG2 cells were treated with 5mM DCA over 72 h (48 h in a 10 cm plate, and the last 24 h in the seahorse plate). To account for differences in cell proliferation, 60.000 cells were seeded per well in the DCA treatment condition, 50.000 in the control conditions the day before glycolysis assay in the Seahorse XF24. The day of the assay the medium was replaced by base DMEM 2mM Glutamine (no FBS, no Glucose, no Pyruvate). After 3 measurements, 20mM Glucose were injected. After 6 measurements 100mM 2DG were injected to completely abrogate glycolysis. The glycolytic rate, or glycolytic capacity, was calculated as the difference between maximal ECAR to basal ECAR. ECAR measurements were normalized with protein concentration (measured by BCA in each well). Statistical analyses were performed with Prism software.

Flow Cytometry:

Briefly, 1 × 106 cells were stained with antibody in PBS with 2% FBS and incubated at 37 °C for 30 min. Cells were then washed and suspended in 200–250 μl PBS 2% FBS and staining was analyzed using a Gallios flow cytometer (Beckman) and the Kaluza software.

Statistical analysis:

The statistical analysis of the difference between means of paired samples was performed using the paired t test. Analysis of multiple comparisons with single control was performed using one-way ANOVA with post-hoc tukey test. The results are given as the confidence interval (*$p < 0.05$, **$p < 0.01$, ***$p < 0.005$). All the experiments described in the figures with a quantitative analysis have been performed at least three times in duplicate. Other experiments were performed three times with similar results

3. Results

3.1. Changes in metabolism regulate expression of proteins involved in lipid uptake through the ERK5 pathway

A successful metabolic switch firstly implies the intake of the new source of energy, e.g. lipids. Secondly the transport to the site where energy must be produced, e.g. the mitochondria. Finally, the organelle must adapt to the new energy production, e.g. FAO. We wished to investigate how inducing a metabolic switch affects these three parameters: cellular uptake, intake in the organelle and metabolic remodeling. We deprived of glucose the OCI-AML3 cells and instead, supplemented the media with galactose, which allows cells to synthesize nucleic acids through the pentose phosphate pathway, and with glutamine, an amino acid that supports oxidative phosphorylation (OXPHOS) [31,32]. The absence of glucose inhibits glycolysis and forces cells to find out an alternative source of energy. In our conditions, OCI-AML3 reacted by increasing the mRNA expression of the FA transporter CD36, as well as its localization at the plasma membrane (Fig. 1A). We found a similar increase in other tumor cell lines, i.e. HuH7, HepG2C and Jurkat, as well as in a primary cell line that we derived from a B-cell lymphoma patient (BCL-P2; Fig. 1A).

Preprints (www.preprints.org) | NOT PEER-REVIEWED | Posted: 8 April 2022 doi:10.20944/preprints202204.0079.v1

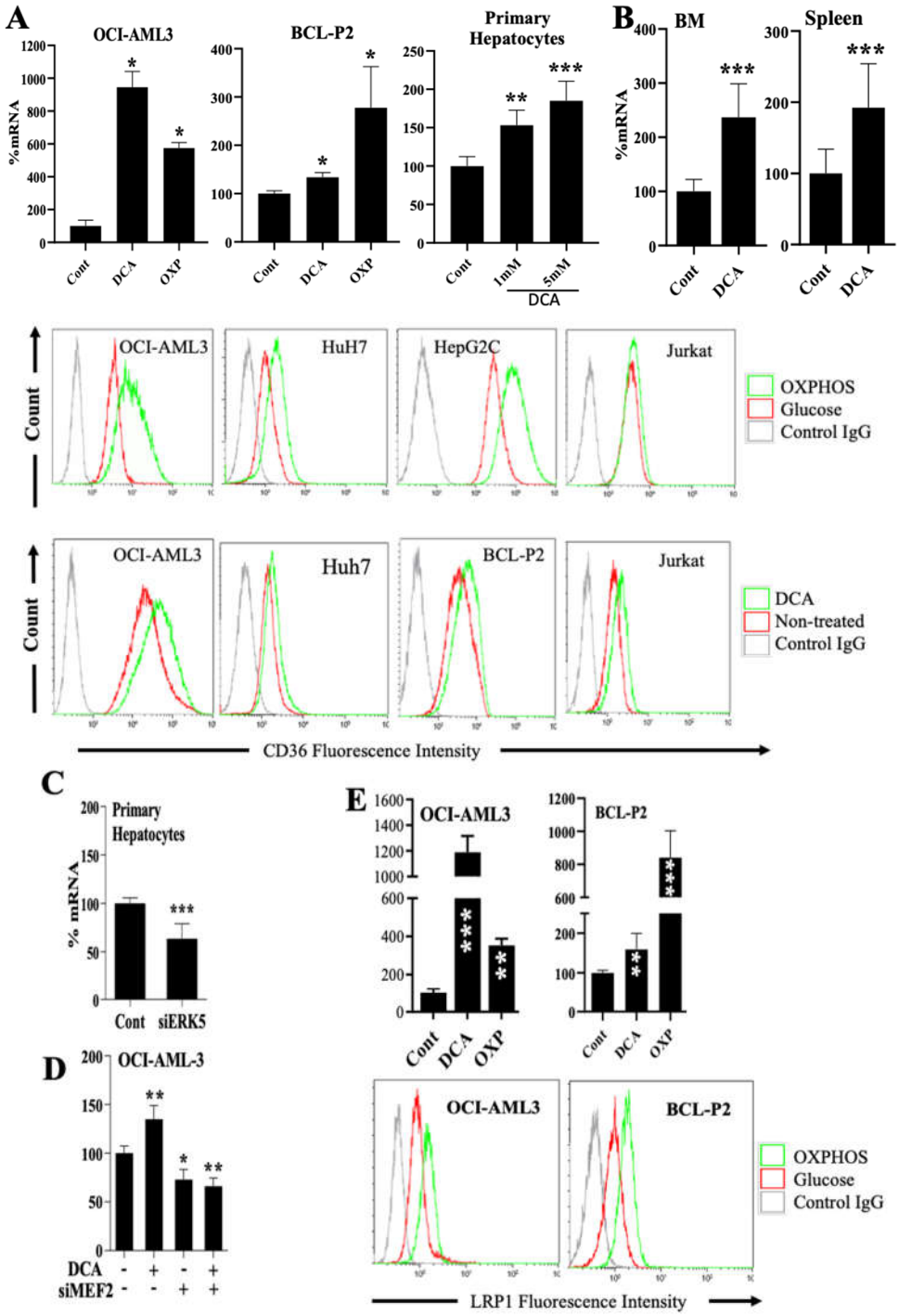

Figure 1. Metabolic changes regulate expression of proteins involved in FA transport through the ERK5/MEF2 pathway. A) CD36 mRNA (up; analyzed by RT-PCR) or CD36 membrane protein (bottom; analyzed by FACs analysis) were analyzed as described in materials and methods section in different cell types treated for 3 days with DCA (5 mM or as indicated) or growing in a glucose-free medium (OXP) that supports OXPHOS for 5-7 days. B) NSG mice were engrafted with primary human AML cells. At day 80 post-graft, they were treated with DCA (n = 4) or leave untreated (n = 4). At day 140, mRNA from bone marrow or spleen was isolated and human CD36 mRNA was quantified by qPCR. C-D) Cells were transfected with plasmids producing siRNA for ERK5 (primary hepatocytes) or MEF2 (OCI-AML cells) and 3 days later we analyzed CD36 mRNA expression. E) Cells were treated as in (A) and LRP1 mRNA (up) or LRP1 membrane protein (bottom) were analyzed as described in (A). Bar graphs represent means ± SD of at least 3 independent experiments performed in triplicate. * p 0.05, ** p 0.01, *** p 0.005 compare to control cells.

 doi:10.20944/preprints202204.0079.v1

We next forced cells to change their metabolism by using the pyruvate dehydrogenase kinase-1 (PDK1) inhibitor dichloroacetate (DCA), which inhibits glycolysis and favors OXPHOS [8,14,33,34]. DCA induced CD36 mRNA and plasma membrane CD36 protein in a large range of tumor cell lines (Fig. 1A and supplemental Fig. 1A-C). DCA also induced CD36 expression in non-transformed cells such as primary hepatocytes (Fig. 1A) and primary natural killer (NK) cells (supplemental Fig. 1A). Notably, prolonged DCA treatment to HepG2C cells for one week further augmented the expression of CD36 on cell surface (supplemental Fig. 1A).

We next engrafted human acute myeloid cells (AML) into NSG mice, which were then treated with DCA as previously described [34]. We isolated bone marrow (BM) and spleen of mice, where AML cells niche, and analyzed CD36 mRNA expression by using qPCR primers specific for human mRNA. DCA increased CD36 mRNA expression of human tumor cells in vivo (Fig. 1B).

We had previously shown that DCA-induced metabolic rewiring requires, at least partially, the activation of the ERK5/MEF2 pathway [14,23,33]. We decreased ERK5 or MEF2 proteins by using small interference RNAs (siRNAs). This effectively reduces ERK5 mRNA and protein between 30 and 70 % in the different cell types used in this study [14,23,33], which we confirmed below in this study (see figure 4E). As previously described, ERK5 has multiple functions, e.g. adaptor, transcriptional activator, kinase, and differences on ERK5 levels can differently affect its effects on the expression of its targets [17–21]. These decrease on expression was similar for MEF2 proteins, although the decrease was bigger for MEF2A than for MEF2C [14,23,33]. siRNA for ERK5 or MEF2 reduced CD36 mRNA expression in resting primary (Fig. 1C) and in transformed (supplemental Fig. 1D) hepatocytes, and in resting or DCA-treated OCI-AML-3 cells (Fig. 1D). ERK5 overexpression in Jurkat cells increased CD36 at the plasma membrane (sup. Fig. 1E). Additionally, chemical inhibition of ERK5 or MEK5, the upstream MAPKK in the ERK5 pathway, decreased CD36 levels in the plasma membrane in several tumor cells (sup. Fig. 1F).

Next, we investigated the effect of metabolic rewiring in the expression of other receptors involved in FA intake. The expression of the scavenger receptor class B type 1 (SCARB1 or CD36L1), which functions as a receptor for high-density lipoprotein (HDL)[35], increased in multiple DCA-treated cells and in cells growing in glucose-free medium (supplemental Fig. 2A). Conversely, ERK5 or MEK5 inhibitors decreased its expression (supplemental Fig. 2B).

CD36 and CD36L1 belong to the low-density lipoprotein receptor-related protein (LRP) family, which also includes LRP1, LRP1B, LRP5, LRP6, LRP10 [36]. Hence, we analyzed if other LRP family members were also regulated by metabolic rewiring. LRP1, which is involved in receptor-mediated endocytosis and lipoprotein metabolism, increased in multiple cell types after metabolic changes similar to those that regulate CD36 and CD36L1 (Fig. 1E and supplemental Fig. 3A), including in vivo, in engrafted AML cells (supplemental Fig. 3B). Conversely, decreasing ERK5 or MEF2 expression, or using ERK5 and MEK5 inhibitors, reduced LRP1 expression (supplemental Fig. 3C). The mRNA of other members of LRP family such as LRP1B, LRP5, LRP6 and LRP10 were equally upregulated by DCA and downregulated by siERK5 (supplemental Fig. 4A). Interestingly, Lipase C (LIPC), hepatic type, which is involved in extracellular lipid metabolism, was equally regulated by DCA treatment or ERK5 levels (supplemental Fig. 4B). This enzyme converts intermediate-density lipoprotein (IDL) to low-density lipoprotein (LDL), and thus plays an important role in the regulation of blood TG levels [37]. Taken together, these results demonstrate that glucose deprivation in cells upregulate the expression of proteins involved in FA uptake at the transcriptional level.

3.2. Changes in metabolism regulate lipid uptake through the ERK5 pathway

Next, we investigated the possible physiological relevance of the increased expression of these proteins involved in FA metabolism. DCA or glucose deprivation increased

Preprints (www.preprints.org) | NOT PEER-REVIEWED | Posted: 8 April 2022 doi:10.20944/preprints202204.0079.v1

cellular uptake of FAs, i.e. dodecanoic and hexadecanoic acids, in HepG2C hepatocytes (Fig. 2A) and in 4 other cell lines (supplemental Fig. 5A). In accordance with mRNA expression, inhibition of ERK5 or MEK5 decreased FA uptake in BCL-P2 cells (Fig. 2B), OCI-AML3 and HepG2 cells (supplemental Fig. 5B).

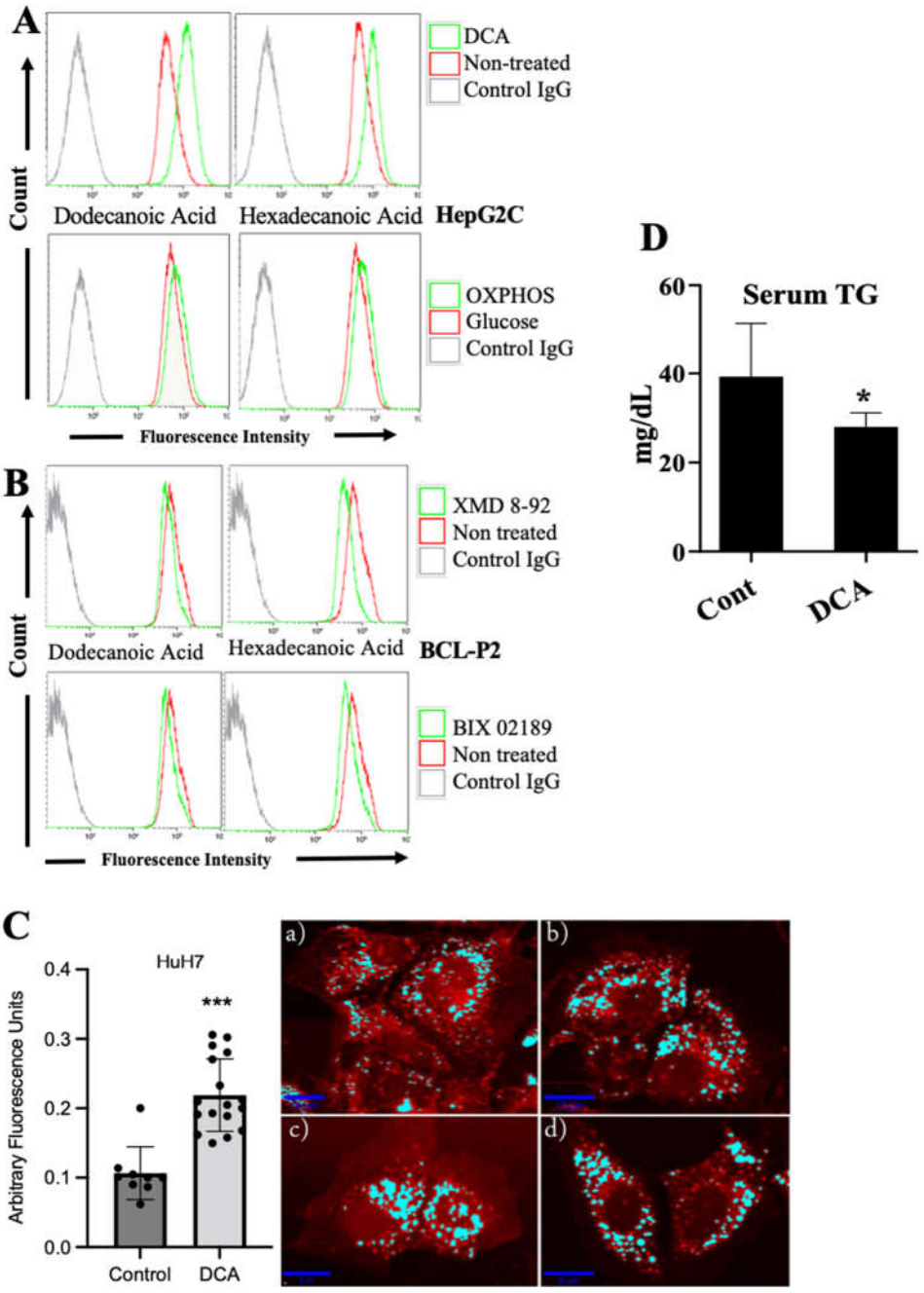

Figure 2. DCA induced intracellular lipid accumulation. A) HepG2 hepatocytes were treated with 5 mM DCA for 3 days or grown in a free-glucose medium that supports OXPHOS for 5-7 days. Cells were incubated for 30 minutes with fluorescent dodecanoic or hexadecanoic FA and the uptake was analyzed by FACs. B) BCL-2 cells were treated with the ERK5 inhibitor XMD 8-92 (10 μM) or with the MEK5 inhibitor BIX 02189 (5 μM) for 24 h before analyzing FA transport. C) HuH7 hepatocytes were grown for 5-7 days without (a-b) or with DCA (c-d) as in (A) and the intracellular amount of lipids were analyzed by Raman microscopy. D) Mice were treated for 4 weeks with DCA (50 mg/kg per day) and the amount of TG measured by multichannel Hitachi Modular analyzer. Bar graphs represent means ± SD of at least 3 independent experiments performed in triplicate. * p 0.05, ** p 0.01, *** p 0.005 compare to control cells.

 doi:10.20944/preprints202204.0079.v1

We further investigated this phenomenon by using a Raman microscope in HuH7 hepatocytes to confirm if metabolic rewiring leads to intracellular lipid accumulation. As expected, we found that DCA treatment in these cells doubled the amount of intracellular lipids (Fig. 2C). Moreover, mice fed for 4 weeks with high fat diet and daily treated with DCA (50 mg/kg) showed decreased blood triglycerides (TG) compared to non-treated mice (Fig. 2D), without affecting body weight or food intake (supplemental Fig. 5C). This further supports the notion that DCA also favors TG intake by cells in vivo.

In summary, these findings suggest that the intake of lipids are largely regulated by metabolic changes through the ERK5 pathway.

3.3. Changes in metabolism regulate the expression of enzymes involved in lipid esterification through the ERK5 pathway

We next analyzed proteins that are involved in FA activation for their use in ATP generation through FAO. The acyl-CoA synthetase long-chain (ACSL) family members catalyze the esterification and activation of the most profuse FA into fatty acyl-CoA and thereby play a key role in their degradation and indirectly promotes their uptake [38]. DCA or glucose-free medium induced ACSL1 mRNA expression in several cell lines and primary transformed and non-transformed cells (Fig. 3A and supplemental Fig. 6A). DCA also increased ACSL1 expression in vivo in AML tumor cells engrafted in NSG mice (Fig. 3B). Decreasing ERK5 or MEF2 mRNA levels with siRNA reduced ACSL1 mRNA in primary hepatocytes (Fig. 3C) and several cell lines (Fig. 3D). This was not specific of ACSL1 because ACSL6 mRNA was equally affected by all these treatments in several cell lines and in primary hepatocytes (Fig. 3E and Supplemental Fig. 6B). These observations suggested that genes involved in lipid esterification were also modulated in an ERK5 dependent fashion in conditions in which glycolysis was suppressed.

Preprints (www.preprints.org) | NOT PEER-REVIEWED | Posted: 8 April 2022 doi:10.20944/preprints202204.0079.v1

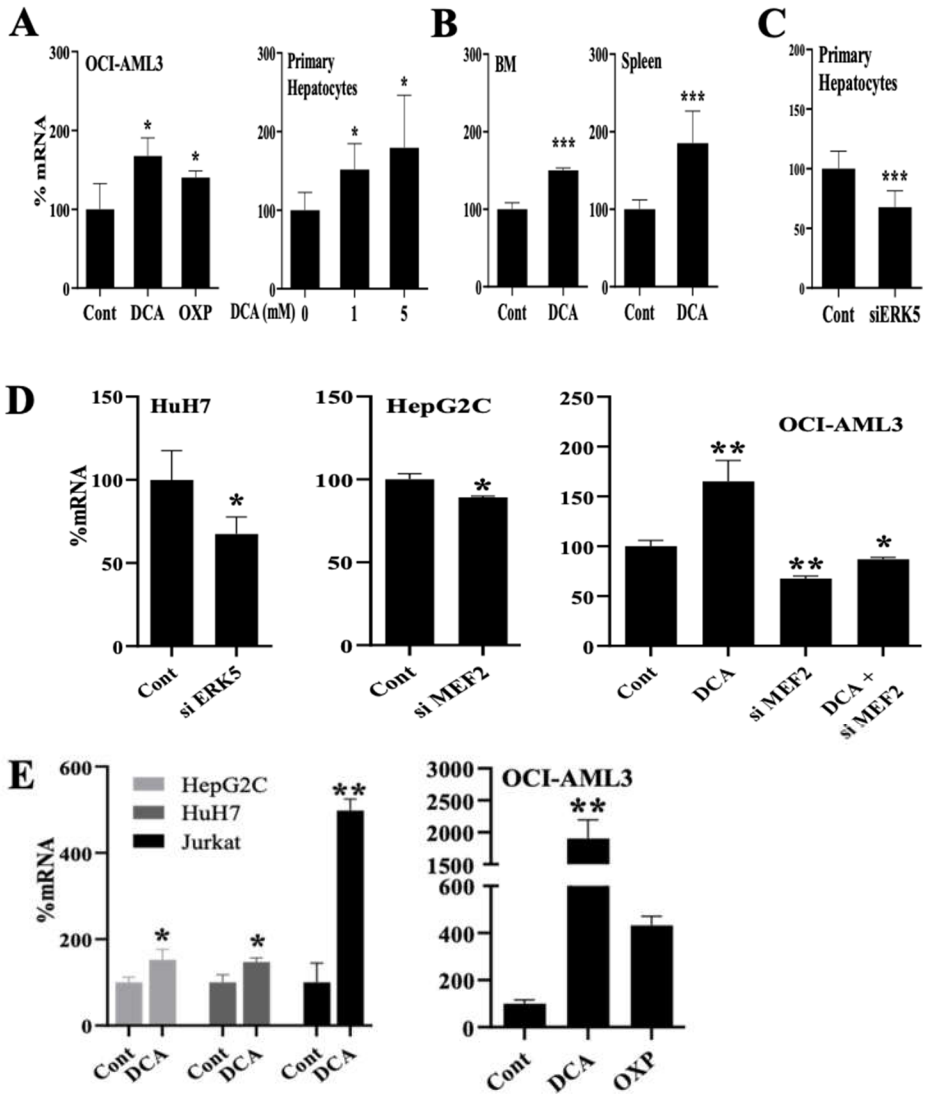

Figure 3. Metabolic changes regulate expression of acyl-CoA synthetase long-chain (ACSL) family members. A) ACSL1 mRNA was analyzed in different cell types treated with DCA (5 mM or as indicated) or growing in a free-glucose medium that induced OXPHOS for 5-7 days. B) NSG mice were grafted with human AML cells and treated with DCA for 16 days before analyzing ACSL1 mRNA expression. C) Primary hepatocytes were transfected with a plasmid producing siRNA for ERK5 and 3 days later we analyzed ACSL1 mRNA expression. D) Different cell types were treated for 72 h with siRNA for ERK5 or MEF2 and treated with 5 mM DCA for 48 hours post-transfection. E) Different cell types were treated as in (D) and ACSL6 mRNA expression was analyzed. Bar graphs represent means ± SD of at least 3 independent experiments performed in triplicate. * p 0.05, ** p 0.01, *** p 0.005 compare to control cells.

3.4. Changes in metabolism regulate FAO through an ERK5-dependent pathway

The acyl-CoA dehydrogenases (ACADs) are enzymes that catalyze the initial step in each cycle of FAO [39]. They are divided in four groups based on their specificity for short (short-chain acyl-CoA dehydrogenase (SCAD), medium (medium-chain acyl-CoA dehydrogenase (ACADM), long-chain (long chain acyl-CoA dehydrogenase (ACADLC) and very long-chain (very long-chain acyl-CoA dehydrogenase (ACADVL) fatty acid acyl-CoA substrates. Hence, ACADVL, which localizes in the inner mitochondrial membrane, plays an essential role in FAO [40]. DCA and glucose-free medium increased expression of ACADVL1 mRNA and protein in several cell types, including primary cells (Fig. 4A-B and supplemental Fig. 7A). DCA also increased ACADVL1 mRNA expression in vivo in AML cells engrafted in NSG mice (Fig. 4C). Moreover, wild-type mice treated for up to 3 days with DCA showed increased Acadvl1 mRNA levels in their liver and spleen (Fig.

Preprints (www.preprints.org) | NOT PEER-REVIEWED | Posted: 8 April 2022 doi:10.20944/preprints202204.0079.v1

4D). Decreasing ERK5 or MEF2 with siRNA reduced ACADVL1 in several cell types (Fig. 4E and supplemental Fig. 7A). Acyl-Coenzyme A dehydrogenase, C-4 to C-12 straight chain (ACADM), which targets medium-chain FA, was equally regulated by DCA, by the absence of glucose or by ERK5 levels (supplemental Fig. 7B).

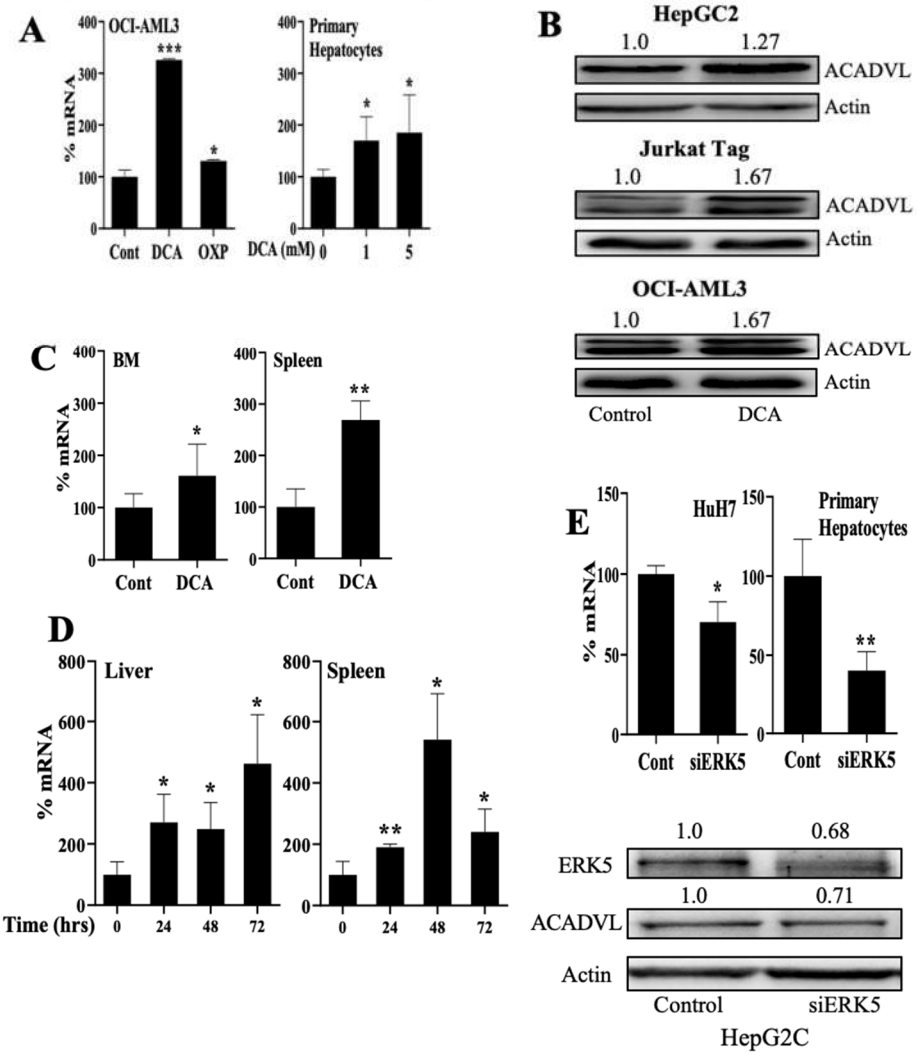

Figure 4. Metabolic changes regulate expression of acyl-CoA dehydrogenases (ACADs) family members. A-B) Different cells were treated with DCA (5 mM or as indicated) or growing in a free-glucose medium that induced OXPHOS for 5-7 days and expression of ACADVL mRNA (A) or protein (B) were analyzed. C) NSG mice were grafted with human AML cells and treated with DCA for 16 days before analyzing ACADVL mRNA expression. D) acadvl mRNA was analyzed in spleen and liver of mice treated for the indicated times with DCA. E) Different hepatic cells were transfected with a plasmid producing siRNA for ERK5 and 3 days later ACADVL mRNA (up) or ACADVL protein (down) were analyzed. Bar graphs represent means ± SD of at least 3 independent experiments performed in triplicate. * p 0.05, ** p 0.01, *** p 0.005 compare to control cells.

As previously discussed, DCA inhibits glycolysis and the results presented above suggested that it induces FAO. In agreement, it increased the basal oxygen consumption rate (OCR; Fig. 5A) and decreased glucose-induced extracellular acidification rate (ECAR; Fig. 5B), likely because it inhibits aerobic glycolysis and this decreases lactate production. In contrast, DCA did not increase maximal respiration (Fig. 5A), suggesting that DCA did not increase mitochondrial mass. Blocking FAO with etomoxir largely decreased basal respiration, showing that HCT116 cells largely depended in FAO (Fig. 5A). DCA could still increase OCR in the presence of etomoxir, hence DCA also increased oxidative phosphorylation (OXPHOS) of other substrates as previously shown [8,14,31,33]. Finally,

Preprints (www.preprints.org) | NOT PEER-REVIEWED | Posted: 8 April 2022 doi:10.20944/preprints202204.0079.v1

etomoxir decreased expression of the FA transporter CD36, CD36L and LRP1 (Fig. 5C), suggesting that inhibition of FAO leads to decrease FA uptake.

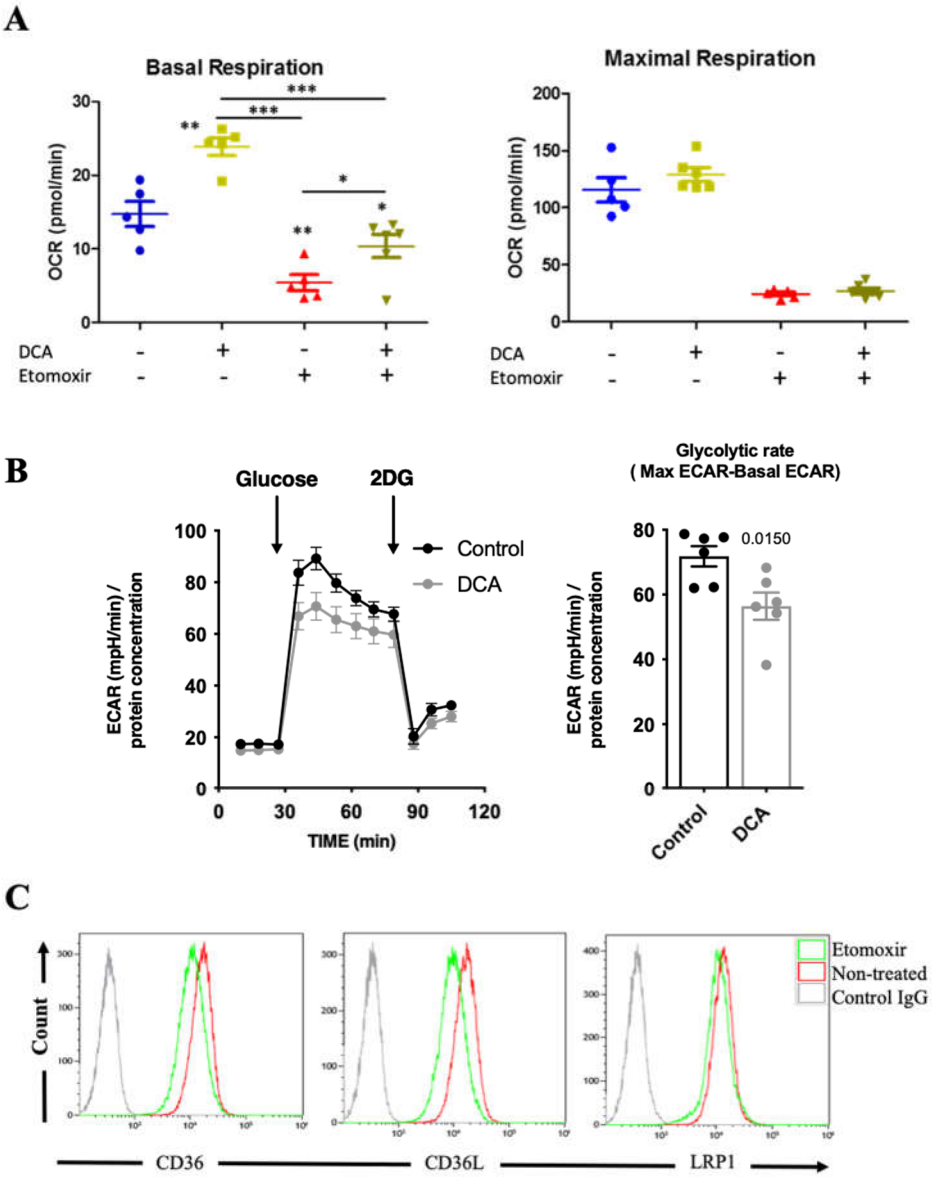

Figure 5. DCA induces FAO. A) HCT 116 cells were incubated with DCA (5 mM) for 3 days and/or etomoxir (5 μM) for 1 hour before analyzing the oxygen consumption (OCR) in basal or maximal respiration in a Seahorse analyzer. Bar graphs represent means ± SD of at least 3 independent experiments performed in triplicate. * p 0.05, ** p 0.01, *** p 0.005 compare to non-treated cells. B) HepG2C cells were incubated with 5 mM DCA over 72 hours (48 hours in a 10 cm plate, and the last 24h in the seahorse plate). To account for differences in cell proliferation, 60.000 cells were seeded per well in the DCA treatment condition, 50.000 in the control conditions the day before a glycolysis assay in a Seahorse XF24. The day of the assay the medium was replaced by base DMEM 2mM Glutamine (no FBS, no Glucose, no Pyruvate). After 3 measurements, 20mM Glucose were injected. After 6 measurements 100mM 2DG were injected to completely abrogate glycolysis. ECAR measurements were normalized with protein concentration (measured by BCA in each well). The glycolytic rate was calculated by subtracting maximal ECAR to basal ECAR. The bar graphs represent means ± SD of 6 independent experiments; Statistics was performed with student t-test compared to non-treated cells. C) Jurkat cells were treated with etomoxir (5 μM) for 24 hours before analyzing by FACs the expression of the depicted proteins.

4. Discussion

 doi:10.20944/preprints202204.0079.v1

Cells should adapt to their environment, which includes substrate availability. This is obvious for unicellular organisms, but it also applies to cells in multicellular beings. After glucose starvation, yeasts shift from glycolysis to fat metabolism thanks to changes in the histone acetylome [4]. Histone acetyltransferases (HATs) are responsible of transferring an acetyl group from acetyl-CoA to histones and histone acetylation is linked to transcriptional activation. Acetyl-CoA is at the junction of many metabolic pathways, enabling it to bring together gene expression and metabolic state. In glucose absence cells shift to an alternative substrate source that, as we show here, can be FAO. This induces high acetyl-CoA levels [41]. DCA induces sustained activation of PDH, which will also increase acetyl-CoA levels [42]. These two mechanisms lead to an acetyl-CoA excess that could change histone acetylation. Previous studies in vivo suggested that DCA has the potential to induce epigenetic remodeling in the heart, which, at least in part, sustains the molecular basis for its therapeutic effect [42]. The ERK5/MEK5 module plays a central role in endothelial cells [43]. This can explain its main role in lipid-related cardiovascular diseases [24,43–46], which could be related to ERK5 control of lipoprotein uptake through LDLR [8]. There are other related receptors that bind to native or modified lipoproteins and that influence diverse physiological or pathological processes [36]. Some of them belong to the LRP family, which includes among others LRP1, LRP1B, LRP5, LRP6, LRP10, CD36 and CD36L [36]. We show here that all these proteins are regulated by ERK5. Interestingly, CD36 activates ERK5 [24], suggesting the presence of a positive feedback loop that supports continuous lipid intake.

ERK5 not only feeds intracellular lipid availability, it also supports lipid esterification by increasing the expression of ACSL enzymes that allow fatty acid activation. Finally, ERK5 also regulates expression of the ACADs, which will start FAO. Therefore, ERK5 sustains a transcriptome remodeling allowing long-term fitness in the new environment [1]. Consequently, we observe that relatively long-term DCA incubation leads to a metabolic rearrangement with cells mainly relying in FAO to obtain energy. In vivo this would lead to lower circulating lipids and could explain the physiological effects of DCA in patients with combined hyperlipoproteinemia or homozygous familial hypercholesterolemia [6,7,10]. Unfortunately for DCA clinical development, it induces neurotoxicity [12,13].

In summary, we show here that different families of enzymes, which are essential to perform FAO, are regulated by the same kinase pathway, i.e. MEK5/ERK5, that transduces changes from the environment to genetic adaptations.

5. Conclusions

Here we show that glucose starvation or sustained pyruvate dehydrogenase (PDH) activation by DCA induce a large genetic remodeling to propel FAO. ERK5 centralizes the remodeling that includes several steps. First, there is an increase in the lipid transport by expression of low-density lipoprotein receptor-related proteins (LRP), e.g. CD36, LRP1 and others. Second, there is an increase on expression of members of the acyl-CoA synthetase long-chain (ACSL) family, which activate FA. Finally, the expression of the enzymes that catalyze the initial step in each cycle of FAO, i.e. the acyl-CoA dehydrogenases (ACADs), is induced. In summary, different families of enzymes, which are essential to perform FAO, are regulated by the same kinase pathway, i.e. MEK5/ERK5, which transduces changes from the environment to genetic adaptations.

Supplementary Materials: It is enclosed in the journal website

Author Contributions: Conceptualization, A.K. and M.V.; methodology, A.K., H.S, C.A., J-M. V., M.B., I.L-M., L.F.,S.G-C., M.D-C. and D.G;; resources, I.L-M and M.V.; writing—original draft preparation, M.V.; funding acquisition, I.L-M and M.V All authors have read and agreed to the published version of the manuscript.

Funding: This work was supported by INCA/DGOS PRT-K program 2021 (MV; 2021-014). AK was recipient of fellowship from Higher Education Commission of Pakistan. This work was also supported by the "Investissements d'avenir" Grant LabEx MAbImprove: ANR-10-LABX-53 (MV).

ICLM is supported by a PRIMA grant from the Swiss National Science Foundation (SNSF PR00P3_193166)

Institutional Review Board Statement: Experimental procedures were conducted according to the European guidelines for animal welfare (2010/63/EU). Protocols were approved by the Animal Care and Use Committee "Languedoc-Roussillon" (approval number: CEEA-LR-12163). All methods were carried out in accordance with the approved guidelines and regulations of this committee.

Data Availability Statement: Not applicable

Acknowledgments: We acknowledge the imaging facility MRI, member of the national infrastructure France-BioImaging supported by the French National Research Agency (ANR-10-INBS-04, «Investments for the future»).

Conflicts of Interest: The authors declare that they have no known competing financial interests or personal relationships that could have appeared to influence the work reported in this paper.

References

1. Ho, W.-C.; Zhang, J. Evolutionary Adaptations to New Environments Generally Reverse Plastic Phenotypic Changes. Nat. Commun. 2018, 9, 350, doi:10.1038/s41467-017-02724-5.
2. Rothman, D.L.; Shulman, R.G. Two Transition States of the Glycogen Shunt and Two Steady States of Gene Expression Support Metabolic Flexibility and the Warburg Effect in Cancer. Neoplasia N. Y. N 2021, 23, 879–886, doi:10.1016/j.neo.2021.06.004.
3. Wolfe, R.R. Metabolic Interactions between Glucose and Fatty Acids in Humans. Am. J. Clin. Nutr. 1998, 67, 519S-526S, doi:10.1093/ajcn/67.3.519S.
4. Hsieh, W.-C.; Sutter, B.M.; Ruess, H.; Barnes, S.D.; Malladi, V.S.; Tu, B.P. Glucose Starvation Induces a Switch in the Histone Acetylome for Activation of Gluconeogenic and Fat Metabolism Genes. Mol. Cell 2022, 82, 60-74.e5, doi:10.1016/j.molcel.2021.12.015.
5. Kankotia, S.; Stacpoole, P.W. Dichloroacetate and Cancer: New Home for an Orphan Drug? Biochim. Biophys. Acta 2014, 1846, 617–629, doi:10.1016/j.bbcan.2014.08.005.
6. Stacpoole, P.W. The Pharmacology of Dichloroacetate. Metabolism 1989, 38, 1124–1144.
7. Moore, G.W.; Swift, L.L.; Rabinowitz, D.; Crofford, O.B.; Oates, J.A.; Stacpoole, P.W. Reduction of Serum Cholesterol in Two Patients with Homozygous Familial Hypercholesterolemia by Dichloroacetate. Atherosclerosis 1979, 33, 285–293.
8. Khan, A.U.H.; Allende-Vega, N.; Gitenay, D.; Gerbal-Chaloin, S.; Gondeau, C.; Vo, D.N.; Belkahla, S.; Orecchioni, S.; Talarico, G.; Bertolini, F.; et al. The PDK1 Inhibitor Dichloroacetate Controls Cholesterol Homeostasis Through the ERK5/MEF2 Pathway. Sci Rep 2017, 7, 10654, doi:10.1038/s41598-017-10339-5.
9. Mainali, R.; Zabalawi, M.; Long, D.; Buechler, N.; Quillen, E.; Key, C.-C.; Zhu, X.; Parks, J.S.; Furdui, C.; Stacpoole, P.W.; et al. Dichloroacetate Reverses Sepsis-Induced Hepatic Metabolic Dysfunction. eLife 2021, 10, e64611, doi:10.7554/eLife.64611.
10. Stacpoole, P.W.; Moore, G.W.; Kornhauser, D.M. Metabolic Effects of Dichloroacetate in Patients with Diabetes Mellitus and Hyperlipoproteinemia — NEJM. N. Engl. J. Med. 1978, 298, 526–530, doi:10.1056/nejm197803092981002.
11. Stacpoole, P.W.; Wright, E.C.; Baumgartner, T.G.; Bersin, R.M.; Buchalter, S.; Curry, S.H.; Duncan, C.A.; Harman, E.M.; Henderson, G.N.; Jenkinson, S. A Controlled Clinical Trial of Dichloroacetate for Treatment of Lactic Acidosis in Adults. The Dichloroacetate-Lactic Acidosis Study Group. N. Engl. J. Med. 1992, 327, 1564–1569, doi:10.1056/NEJM199211263272204.
12. Kaufmann, P.; Engelstad, K.; Wei, Y.; Jhung, S.; Sano, M.C.; Shungu, D.C.; Millar, W.S.; Hong, X.; Gooch, C.L.; Mao, X.; et al. Dichloroacetate Causes Toxic Neuropathy in MELAS: A Randomized, Controlled Clinical Trial. Neurology 2006, 66, 324–330, doi:10.1212/01.wnl.0000196641.05913.27.
13. Felitsyn, N.; Stacpoole, P.W.; Notterpek, L. Dichloroacetate Causes Reversible Demyelination in Vitro: Potential Mechanism for Its Neuropathic Effect. J. Neurochem. 2007, 100, 429–436, doi:10.1111/j.1471-4159.2006.04248.x.
14. Khan, A.U.H.; Allende-Vega, N.; Gitenay, D.; Garaude, J.; Vo, D.N.; Belkhala, S.; Gerbal-Chaloin, S.; Gondeau, C.; Daujat-Chavanieu, M.; Delettre, C.; et al. Mitochondrial Complex I Activity Signals Antioxidant Response through ERK5. Sci Rep 2018, 8, 7420, doi:10.1038/s41598-018-23884-4.
15. Belkahla, S.; Haq Khan, A.U.; Gitenay, D.; Alexia, C.; Gondeau, C.; Vo, D.N.; Orecchioni, S.; Talarico, G.; Bertolini, F.; Cartron, G.; et al. Changes in Metabolism Affect Expression of ABC Transporters through ERK5 and Depending on P53 Status. Oncotarget 2018, 9, 1114–1129, doi:10.18632/oncotarget.23305.
16. Khan, A.U.H.; Rathore, M.G.; Allende-Vega, N.; Vo, D.N.; Belkhala, S.; Orecchioni, S.; Talarico, G.; Bertolini, F.; Cartron, G.; Lecellier, C.H.; et al. Human Leukemic Cells Performing Oxidative Phosphorylation (OXPHOS) Generate an Antioxidant Response Independently of Reactive Oxygen Species (ROS) Production. EBioMedicine 2016, 3, 43–53, doi:10.1016/j.ebiom.2015.11.045 S2352-3964(15)30228-0 [pii].
17. Barsyte-Lovejoy, D.; Galanis, A.; Clancy, A.; Sharrocks, A.D. ERK5 Is Targeted to Myocyte Enhancer Factor 2A (MEF2A) through a MAPK Docking Motif. Biochem J 2004, 381, 693–699.
18. Kato, Y.; Kravchenko, V.V.; Tapping, R.I.; Han, J.; Ulevitch, R.J.; Lee, J.D. BMK1/ERK5 Regulates Serum-Induced Early Gene Expression through Transcription Factor MEF2C. Embo J 1997, 16, 7054–7066.

19. Young, A.; Wu, W.; Sun, W.; Benjamin Larman, H.; Wang, N.; Li, Y.S.; Shyy, J.Y.; Chien, S.; Garcia-Cardena, G. Flow Activation of AMP-Activated Protein Kinase in Vascular Endothelium Leads to Kruppel-like Factor 2 Expression. Arter. Thromb Vasc Biol 2009, 29, 1902–1908, doi:10.1161/ATVBAHA.109.193540.
20. Monti, M.; Celli, J.; Missale, F.; Cersosimo, F.; Russo, M.; Belloni, E.; Di Matteo, A.; Lonardi, S.; Vermi, W.; Ghigna, C.; et al. Clinical Significance and Regulation of ERK5 Expression and Function in Cancer. Cancers 2022, 14, 348, doi:10.3390/cancers14020348.
21. Kasler, H.G.; Victoria, J.; Duramad, O.; Winoto, A. ERK5 Is a Novel Type of Mitogen-Activated Protein Kinase Containing a Transcriptional Activation Domain. Mol Cell Biol 2000, 20, 8382-9.
22. Stecca, B.; Rovida, E. Impact of ERK5 on the Hallmarks of Cancer. Int. J. Mol. Sci. 2019, 20, E1426, doi:10.3390/ijms20061426.
23. Khan, A.U.H.; Allende-Vega, N.; Gitenay, D.; Gerbal-Chaloin, S.; Gondeau, C.; Vo, D.N.; Belkahla, S.; Orecchioni, S.; Talarico, G.; Bertolini, F.; et al. The PDK1 Inhibitor Dichloroacetate Controls Cholesterol Homeostasis Through the ERK5/MEF2 Pathway. Sci Rep 2017, 7, 10654, doi:10.1038/s41598-017-10339-5.
24. Yang, M.; Cooley, B.C.; Li, W.; Chen, Y.; Vasquez-Vivar, J.; Scoggins, N.O.; Cameron, S.J.; Morrell, C.N.; Silverstein, R.L. Platelet CD36 Promotes Thrombosis by Activating Redox Sensor ERK5 in Hyperlipidemic Conditions. Blood 2017, 129, 2917–2927, doi:10.1182/blood-2016-11-750133.
25. Cristea, S.; Coles, G.L.; Hornburg, D.; Gershkovitz, M.; Arand, J.; Cao, S.; Sen, T.; Williamson, S.C.; Kim, J.W.; Drainas, A.P.; et al. The MEK5-ERK5 Kinase Axis Controls Lipid Metabolism in Small-Cell Lung Cancer. Cancer Res. 2020, 80, 1293–1303, doi:10.1158/0008-5472.CAN-19-1027.
26. Nigro, P.; Abe, J.; Berk, B.C. Flow Shear Stress and Atherosclerosis: A Matter of Site Specificity. Antioxid Redox Signal 2011, 15, 1405–1414.
27. Kim, M.; Kim, S.; Lim, J.H.; Lee, C.; Choi, H.C.; Woo, C.H. Laminar Flow Activation of ERK5 Protein in Vascular Endothelium Leads to Atheroprotective Effect via NF-E2-Related Factor 2 (Nrf2) Activation. J Biol Chem 2012, 287, 40722–40731, doi:10.1074/jbc.M112.381509.
28. Allende-Vega, N.; Marco Brualla, J.; Falvo, P.; Alexia, C.; Constantinides, M.; de Maudave, A.F.; Coenon, L.; Gitenay, D.; Mitola, G.; Massa, P.; et al. Metformin Sensitizes Leukemic Cells to Cytotoxic Lymphocytes by Increasing Expression of Intercellular Adhesion Molecule-1 (ICAM-1). Sci. Rep. 2022, 12, 1341, doi:10.1038/s41598-022-05470-x.
29. Pichard, L.; Raulet, E.; Fabre, G.; Ferrini, J.B.; Ourlin, J.C.; Maurel, P. Human Hepatocyte Culture. Methods Mol Biol 2006, 320, 283–293, doi:10.1385/1-59259-998-2:283.
30. Garaude, J.; Cherni, S.; Kaminski, S.; Delepine, E.; Chable-Bessia, C.; Benkirane, M.; Borges, J.; Pandiella, A.; Iniguez, M.A.; Fresno, M.; et al. ERK5 Activates NF-KappaB in Leukemic T Cells and Is Essential for Their Growth in Vivo. J Immunol 2006, 177, 7607–7617.
31. Charni, S.; de Bettignies, G.; Rathore, M.G.; Aguilo, J.I.; van den Elsen, P.J.; Haouzi, D.; Hipskind, R.A.; Enriquez, J.A.; Sanchez-Beato, M.; Pardo, J.; et al. Oxidative Phosphorylation Induces de Novo Expression of the MHC Class I in Tumor Cells through the ERK5 Pathway. J Immunol 2010, 185, 3498–3503.
32. Fan, J.; Kamphorst, J.J.; Mathew, R.; Chung, M.K.; White, E.; Shlomi, T.; Rabinowitz, J.D. Glutamine-Driven Oxidative Phosphorylation Is a Major ATP Source in Transformed Mammalian Cells in Both Normoxia and Hypoxia. Mol. Syst. Biol. 2013, 9, 712, doi:10.1038/msb.2013.65.
33. Khan, A.U.; Rathore, M.G.; Allende-Vega, N.; Vo, D.N.; Belkhala, S.; Orecchioni, S.; Talarico, G.; Bertolini, F.; Cartron, G.; Lecellier, C.H.; et al. Human Leukemic Cells Performing Oxidative Phosphorylation (OXPHOS) Generate an Antioxidant Response Independently of Reactive Oxygen Species (ROS) Production. EBioMedicine 2016, 3, 43–53, doi:10.1016/j.ebiom.2015.11.045.
34. Allende-Vega, N.; Krzywinska, E.; Orecchioni, S.; Lopez-Royuela, N.; Reggiani, F.; Talarico, G.; Rossi, J.F.; Rossignol, R.; Hicheri, Y.; Cartron, G.; et al. The Presence of Wild Type P53 in Hematological Cancers Improves the Efficacy of Combinational Therapy Targeting Metabolism. Oncotarget 2015, 6, 19228–19245.
35. Acton, S.; Rigotti, A.; Landschulz, K.T.; Xu, S.; Hobbs, H.H.; Krieger, M. Identification of Scavenger Receptor SR-BI as a High Density Lipoprotein Receptor. Science 1996, 271, 518–520, doi:10.1126/science.271.5248.518.
36. Mineo, C. Lipoprotein Receptor Signalling in Atherosclerosis. Cardiovasc. Res. 2020, 116, 1254–1274, doi:10.1093/cvr/cvz338.
37. Nilsson-Ehle, P.; Garfinkel, A.S.; Schotz, M.C. Lipolytic Enzymes and Plasma Lipoprotein Metabolism. Annu. Rev. Biochem. 1980, 49, 667–693, doi:10.1146/annurev.bi.49.070180.003315.
38. Tang, Y.; Zhou, J.; Hooi, S.C.; Jiang, Y.-M.; Lu, G.-D. Fatty Acid Activation in Carcinogenesis and Cancer Development: Essential Roles of Long-Chain Acyl-CoA Synthetases. Oncol. Lett. 2018, 16, 1390–1396, doi:10.3892/ol.2018.8843.
39. Wajner, M.; Amaral, A.U. Mitochondrial Dysfunction in Fatty Acid Oxidation Disorders: Insights from Human and Animal Studies. Biosci. Rep. 2015, 36, e00281, doi:10.1042/BSR20150240.
40. Yamada, K.; Taketani, T. Management and Diagnosis of Mitochondrial Fatty Acid Oxidation Disorders: Focus on Very-Long-Chain Acyl-CoA Dehydrogenase Deficiency. J. Hum. Genet. 2019, 64, 73–85, doi:10.1038/s10038-018-0527-7.
41. Ma, Y.; Temkin, S.M.; Hawkridge, A.M.; Guo, C.; Wang, W.; Wang, X.-Y.; Fang, X. Fatty Acid Oxidation: An Emerging Facet of Metabolic Transformation in Cancer. Cancer Lett. 2018, 435, 92–100, doi:10.1016/j.canlet.2018.08.006.

42. Matsuhashi, T.; Hishiki, T.; Zhou, H.; Ono, T.; Kaneda, R.; Iso, T.; Yamaguchi, A.; Endo, J.; Katsumata, Y.; Atsushi, A.; et al. Activation of Pyruvate Dehydrogenase by Dichloroacetate Has the Potential to Induce Epigenetic Remodeling in the Heart. J. Mol. Cell. Cardiol. 2015, 82, 116–124, doi:10.1016/j.yjmcc.2015.02.021.
43. Hayashi, M.; Kim, S.W.; Imanaka-Yoshida, K.; Yoshida, T.; Abel, E.D.; Eliceiri, B.; Yang, Y.; Ulevitch, R.J.; Lee, J.D. Targeted Deletion of BMK1/ERK5 in Adult Mice Perturbs Vascular Integrity and Leads to Endothelial Failure. J Clin Invest 2004, 113, 1138–1148.
44. Liu, W.; Ruiz-Velasco, A.; Wang, S.; Khan, S.; Zi, M.; Jungmann, A.; Dolores Camacho-Munoz, M.; Guo, J.; Du, G.; Xie, L.; et al. Metabolic Stress-Induced Cardiomyopathy Is Caused by Mitochondrial Dysfunction Due to Attenuated Erk5 Signaling. Nat Commun 2017, 8, 494, doi:10.1038/s41467-017-00664-8.
45. Regan, C.P.; Li, W.; Boucher, D.M.; Spatz, S.; Su, M.S.; Kuida, K. Erk5 Null Mice Display Multiple Extraembryonic Vascular and Embryonic Cardiovascular Defects. Proc Natl Acad Sci U A 2002, 99, 9248–9253.
46. Sohn, S.J.; Sarvis, B.K.; Cado, D.; Winoto, A. ERK5 MAPK Regulates Embryonic Angiogenesis and Acts as a Hypoxia-Sensitive Repressor of Vascular Endothelial Growth Factor Expression. J Biol Chem 2002, 277, 43344–43351.